International Journal of Mechanical Sciences 81 (2014) 77–87

Contents lists available at ScienceDirect

International Journal of Mechanical Sciences

journal homepage: www.elsevier.com/locate/ijmecsci

Numerical contribution to the comprehension of saw-toothed Ti6Al4V chip formation in orthogonal cutting

F. Ducobu *, E. Rivière-Lorphèvre, E. Filippi

University of Mons (UMONS), Faculty of Engineering (FPMs), Machine Design and Production Engineering Department, 20 Place du Parc, B-7000 Mons, Belgium

ARTICLE INFO

Article history:
Received 19 October 2013
Received in revised form
23 January 2014
Accepted 12 February 2014
Available online 19 February 2014

Keywords:
Abaqus/explicit
Finite element model
Orthogonal cutting
Saw-toothed chip
Teeth formation frequency
Titanium alloy Ti6Al4V

ABSTRACT

The physics of formation of a saw-toothed (or segmented) Ti6Al4V chip in machining is still an ongoing issue in the literature as well as its modelling and numerical simulation. After a review of the theories explaining the formation of such a chip, three finite element models are presented with a desire to take into account the physical phenomena. The results of the simulations are compared with the different theories reported in the literature. This confrontation allows us to keep the most relevant model which contributes to the understanding of the phenomena. It shows that combining the adiabatic shear band and the crack propagation leads to a chip morphology and formation mechanism close to the experimental one. The study also allows to estimate the teeth formation frequency of the numerical chip.

1. Introduction

Titanium alloy machined parts are commonly used by aerospace and biomedical companies to get high mechanical, fatigue and corrosion resistances coupled with a low mass and a good biocompatibility [1]. Unfortunately its low thermal conductivity coupled with hardening makes it a difficult-to-machine material. Barry et al. [2] show that these factors contribute to the formation of a saw-toothed chip in many cutting conditions.

The phenomena leading to the formation of a saw-toothed (also called segmented, serrated or fragmented in the literature) Ti6Al4V chip are still an ongoing issue in the literature up to now. However in addition to experimental tests, numerical modelling can be used to help the scientific community to understand these phenomena and to predict the cutting conditions leading to such a chip.

This study takes place in the numerical aspects of the problem in which there is still much efforts to do before being able to have models accurately reproducing the chip morphology and all the physical phenomena involved in its formation.

The paper begins with a brief literature review of the different theories leading to the formation of a saw-toothed Ti6Al4V chip. The finite element models developed and their results are then presented. The common thread in the development of these models is the link with the physical phenomena and the absence of numerical tricks. Model results are then used to compare the different theories identified in the literature. The model leading to results closer to the experimental reference is kept for a more detailed analysis before concluding on the whole paper.

2. Literature review

Three theories about the formation of a saw-toothed chip coexist in the current literature. The first one is the adiabatic shear band, while the second one introduces crack propagation within the primary shear zone. Some authors combine them in a third one to explain the formation of this kind of chips. Each one will be briefly presented in the following paragraphs.

2.1. Adiabatic shear band

Molinari et al. [3] define the adiabatic shear band as the outward of a thermoplastic instability in the primary shear zone and observed the influence of the cutting speed on adiabatic shear bands. In the case of a saw-toothed chip, large shear strains appear in very thin bands. These strain localisations induce a very large local temperature increase, which is a necessary condition to get an adiabatic shear. Owen and Vaz [4] notice that the formation of a saw-toothed Ti6Al4V chip by the adiabatic shear band theory is favoured by its thermomechanical properties (low thermal conductivity, specific mass, specific heat and limit of

* Corresponding author. Tel.: +32 65 45 47; fax: +32 65 45 45.
E-mail address: Francois.Ducobu@umons.ac.be (F. Ducobu).

http://dx.doi.org/10.1016/j.ijmecsci.2014.02.017
0020-7403

elasticity sensitive to temperature). According to Fourment and Delalondre [5], this adiabatic shear band is the result of a competition between hardening and strain softening. They suggest that a tooth is formed when the strain softening becomes dominant. The action of the strain softening would therefore be necessary to form a saw-toothed Ti6Al4V chip.

Modellings of Bäker et al. [6] show that the shear band starts near the cutting edge radius of the tool, then a second one begins to form at the free chip surface before the first one has the time to extend on all the width of the shear zone. Then the two join to form a complete shear band. They also observed that the shear band can split in the cutting edge radius zone (Fig. 1). These observations were confirmed experimentally.

According to Komanduri and Turkovich [7], Komanduri [8] and Hou and Komanduri [9], the formation of an adiabatic shear band (which they call "catastrophic shear") implies a plastic instability but also a stick and slip motion of the chip with respect to the surface of the tool.

2.2. Formation by crack propagation

Vyas and Shaw [10] experimentally observed a continuous crack starting from the free chip surface and propagating in the primary shear zone. From about the half of the width of the shear zone the crack begins to be discontinuous. The localised and disconnected resulting cracks are called "micro-cracks".

Hua and Shivpuri [11] noticed during their numerical simulations a crack initiation within the primary shear zone.

2.3. Formation by adiabatic shear band and crack propagation

The third theory is a combination of the two previous ones, as shown in Fig. 2.

Bai and Dodd [13] suggest that the adiabatic shear band is the precursor of failure. According to Owen and Vaz [4] and Giovanola [14], material failure in the shear zone occurs in two steps: the thermal softening, followed by failure (via nucleation, growth and coalescence of voids), which constitutes the main mechanism of the material failure. Seshacharyulu et al. [15] observe experimentally that cracking occurs along adiabatic shear bands at temperatures lower than 800 °C and strain rates larger than 1 s^{-1}; these conditions are fulfilled in the primary shear zone.

Calamaz et al. [16] present a numerical finite element model taking into account the strain softening of Ti6Al4V thanks to the introduction of the Hyperbolic TANgent (TANH) law [17,18], a modified Johnson–Cook (J–C) law. They observed that adding a damage criterion allows them to predict a saw-toothed chip geometrically closer to the experimental one.

Sima and Özel [19] also developed a TANH model very similar to that of Calamaz et al. which adds a parameter allowing further control on the softening part of the stress–strain curve. This work studies the effect of the strain softening model on the adiabatic shear band formation, complementing and confirming the results of Calamaz et al.

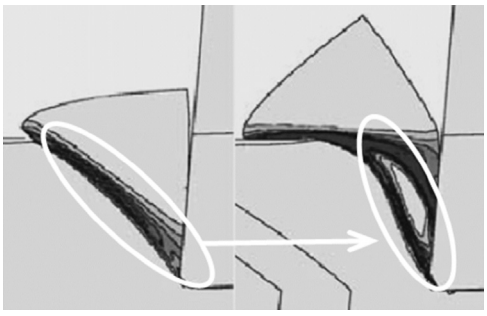

Fig. 1. Modelled split shear band in Ti6Al4V, adapted from Bäker et al. [6].

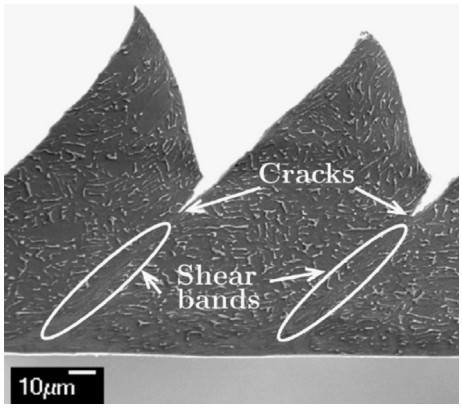

Fig. 2. Saw-toothed Ti6Al4V chip illustrating the third theory, adapted from Castro [12].

2.4. Conclusions of the literature review

Three competing theories can currently be found in the literature. They are the adiabatic shear band, the crack propagation and the combination of the two first theories.

Numerical simulations of Calamaz et al. [16] show that the adiabatic shear band alone may allow the formation of a saw-toothed chip but the addition of a damage criterion leads to a saw-toothed chip with a geometry closer to the one obtained by experiments.

The following part of this paper will focus on the numerical modelling of orthogonal cutting of Ti6Al4V. It will numerically contribute to the understanding of the phenomena involved in the formation of such chips.

3. Ti6Al4V saw-toothed chip formation with the finite element method

Three different models are considered to simulate the formation of a saw-toothed Ti6Al4V chip in orthogonal cutting. The models were developed (with the commercial software ABAQUS/Explicit v6.8) so that the three theories explaining the formation of a Ti6Al4V saw-toothed chip can be investigated. They consist of combinations of the two formalisms, Arbitrary Lagrangian Eulerian (ALE) and Lagrangian, and the two constitutive laws, Johnson–Cook law [20] and TANH law [16], chosen to represent the behaviour of Ti6Al4V:

- First theory: ALE with TANH law (ALETANH), taking only strain softening into account.
- Second theory: Lagrangian with Johnson–Cook law (LJC), taking only crack propagation into account.
- Third theory: Lagrangian with TANH law (LTANH), taking crack propagation and strain softening into account.

These three models consist of 2D plane strain orthogonal cutting models focusing on the area close to the cutting edge of the tool. They were developed with a desire to respect the physical phenomena and to avoid the introduction of numerical tricks, very frequent in numerical modelling.

In order to compare modelled cutting forces and chip morphologies to experimental data, the cutting conditions are as close as possible to those of the reference article of Sun et al. [21]. These authors performed turning experiments on mill annealed Ti6Al4V

bars (diameter of 60 mm) by dry machining and forces were measured with a 3-component force sensor (PCB Model 260A1).

3.1. Initial geometry and boundary conditions

Fig. 3 presents a schematical representation of the initial geometry and boundary conditions of the models.

The workpiece is modelled as rectangular block of 1.5 mm long and 1 mm wide. The tool has an edge radius of 20 µm, a rake angle of 15° and a clearance angle of 2°. The depth of cut, h, is equal to 0.28 mm.

Concerning the boundary conditions, the workpiece is fixed in space while the tool moves towards the workpiece at the cutting speed, v_c, of 75 m/min.

3.2. Material constitutive models and properties

3.2.1. Workpiece

Two laws are considered to describe the workpiece material (Ti6Al4V) behaviour: the Johnson–Cook law [20] and the TANH law [16], depending on the model. Model results will help to choose the best suited for Ti6Al4V saw-toothed chip formation.

The Johnson–Cook law [20] is the most popular constitutive model used in cutting process simulation. It dissociates plastic, viscous and thermal aspects in three independent terms:

$$\sigma = (A+B\varepsilon^n)\left(1+C\ln\frac{\dot{\varepsilon}}{\dot{\varepsilon}_0}\right)\left(1-\left[\frac{T-T_{room}}{T_{melt}-T_{room}}\right]^m\right) \quad (1)$$

where T_{melt} is the melting temperature, T_{room} is the room temperature (298 K, in this paper) and $\dot{\varepsilon}_0$ is the reference strain rate. A, B, C, m and n are material properties.

An important advantage of this law is the large amount of available parameters for many materials. But it can also be a weakness: many possibilities are available and determining the right one is not easy (a synthesis for Ti6Al4V is performed by Ducobu [22]). Table 1 presents the set used for this study. According to Meyer and Kleponis [23], the parameters were determined at strain rate levels of 0.0001 s^{-1}, 0.1 s^{-1} and 2150 s^{-1} and at a maximum plastic strain of 0.57. These Johnson–Cook parameters were selected for this study as the value of parameter A, 862 MPa, is equal to the yield stress of Ti6Al4V at room temperature [16]. It was furthermore estimated as the most popular and frequently found in the literature.

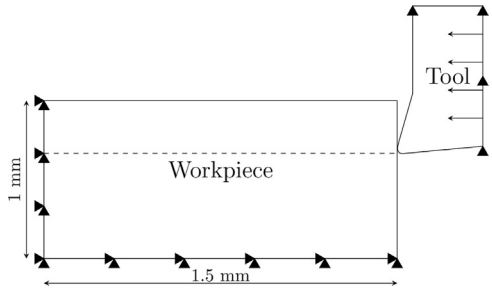

Fig. 3. Initial geometry and boundary conditions of the models.

Table 1
Parameters of the Johnson–Cook law for Ti6Al4V, from [24–27] (among others).

J–C law parameters	
A (MPa)	862
B (MPa)	331
C	0.012
m	0.8
n	0.34
T_{melt} (K)	1878

According to Calamaz et al. [16], the Johnson–Cook law correctly represents the behaviour of the material up to strain rates of 1000 s^{-1} and strains of about 0.3. These values are smaller than these encountered in machining: strain can be as large as 6 and strain rates as 10^7 s^{-1} [28]. Moreover strains larger than 0.5 would lead to the strain softening phenomenon, which was identified in the literature review as one of the causes responsible for the formation of saw-toothed Ti6Al4V chips. The physical phenomena at the origin of this softening are not yet known but dynamic recrystallisation (mainly in the β phase field) could be the main reason according to Ding et al. [29].

In order to introduce this strain softening in the material behaviour, Calamaz et al. [16] propose to upgrade the Johnson–Cook law to the Hyperbolic TANgent law. A more realistic chip should therefore be formed thanks to this law.

Fig. 4 presents the comparison between the Johnson–Cook law and the TANH law. In this figure, there is no experimental curve to appreciate the benefit of the TANH law, as this information is not available. Indeed, today's experimental technology does not allow us to reach sufficiently high strains and strain rates, moreover at high temperatures, to highlight the strain softening. For example, Lee and Lin [30] provide experimental curves for strains up to only 0.25 (which is too low to measure the strain softening) and strain rates of 2000 s^{-1} at temperatures between 973 K and 1373 K.

The TANH law is expressed by the following equation [16]:

$$\sigma = \left[A+B\,\varepsilon^n\left(\frac{1}{\exp(\varepsilon^a)}\right)\right]\left[1+C\ln\frac{\dot{\varepsilon}}{\dot{\varepsilon}_0}\right]\left[1-\left(\frac{T-T_{room}}{T_{melt}-T_{room}}\right)^m\right]\left[D+(1-D)\tanh\left(\frac{1}{(\varepsilon+S)^c}\right)\right] \quad (2)$$

with

$$D = 1-\left(\frac{T}{T_{melt}}\right)^d \quad \text{and} \quad S = \left(\frac{T}{T_{melt}}\right)^b$$

Parameters A, B, C, m and n have the same meaning as for Johnson–Cook, while a, b, c and d are the new constants introduced by the TANH law.

The parameter values are given in Table 2. These values were obtained by Calamaz et al. [16] through inverse analysis on their numerical results. The analysis was performed by comparison with the experimental results on the global morphology of the chips, the cutting forces and geometrical characteristics of the chips.

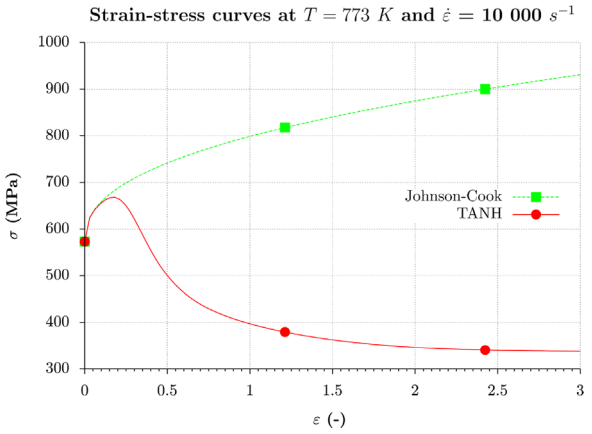

Fig. 4. Comparison of the shapes of Johnson–Cook and TANH laws.

Table 2
Parameters of the TANH law for Ti6Al4V, from [16].

TANH law parameters			
A (MPa)	968	a	1.6
B (MPa)	380	b	0.4
C	0.02	c	6
m	0.577	d	1
n	0.421		
T_{melt} (K)	1878		

Table 3
Materials properties, from [24,26,27,31].

Material properties	Ti6Al4V	WC
Density (kg/m^3)	4430	15,000
Young's modulus (GPa)	113.8	800
Poisson's ratio (–)	0.342	0.2
Expansion (m/m K)	8.6e^{-6}	4.7e^{-6}
Thermal conductivity (W/m K)	7.3	46
Specific heat (J/kg/K)	580	203

3.2.2. Other mechanical properties

The tool material (tungsten carbide) is also considered as homogeneous and its behaviour is described by a linear elastic law.

The numerical values of the materials properties can be found in Table 3.

3.3. Contact and friction modelling

The tool–workpiece contact is defined between the outer surface of the tool and all the nodes of the workpiece. It is necessary to consider all the nodes of the workpiece since the chip formation must not be influenced or favoured. Moreover, as the tool advances, it is in contact with nodes that were originally inside the workpiece. This constitutes an additional difficulty in managing contact interactions.

Coulomb's friction, with a low coefficient value (0.05), is used to model friction at the tool–workpiece interface in accordance with Bäker et al. [6] and Calamaz et al. [16].

All the energy generated by friction is converted into heat, as usually assumed [32].

3.4. Thermal aspects

Only conduction is considered and all the parts faces are adiabatic because the simulation time is short (less than a millisecond) and the heat does not have the time to spread to the geometrical limits of the models.

It is assumed that the transformation of the deformation to heat occurs with an efficiency of 90%, assumption usually applied [24,32,33].

3.5. Formalisms adopted

Two types of formulations were envisaged to model the Ti6Al4V saw-toothed chip formation in orthogonal cutting: ALE and Lagrangian. The specificities of each are outlined in this paragraph.

3.5.1. ALE

Models developed with the ALE formalism do not use a chip separation criterion, as it is considered that the chip formation is due to plastic flow of material around the tool [33]. The absence of such a criterion is a benefit from a numerical point of view but its physical validity could be questioned.

The tool is meshed with three- and four-nodes plane strain elements with linear displacement and temperature formulation, while the part is meshed with only four-nodes square elements. The upper part of the workpiece is meshed more finely (element length of 5 μm) in order to take into account the tool edge radius. Indeed, as it has a value of 20 μm, it is crucial that the elements with which it interacts are smaller than 20 μm. Taking into account the tool edge radius introduces difficulties related to the flattening of the mesh elements located close to it. The tool is therefore often considered as sharp or the geometry of the workpiece is adapted to avoid this problem (for example, Mabrouki et al. [34] add a chamfer on the workpiece).

3.5.2. Lagrangian

Due to the Lagrangian formulation, a chip separation criterion must be introduced in the model. This chip separation criterion is a key parameter to obtain realistic simulations, as highlighted by Pantalé [28].

As stated in the objectives of this paper, the chip formation cannot be influenced or favoured. The method imposing a line along which the material separate to form the chip is therefore prohibited. The criterion adopted is an “eroding” elements method with crack propagation in the workpiece.

The proposed separation criterion is based on the temperature dependent tensile failure (hydrostatic pressure stress, [35]) of Ti6Al4V. This is in accordance with Lorentzon et al. [36] who showed for Inconel 718 that the fracture criterion should have a hydrostatic dependency to model accurately the formation of a chip that is not continuous. As soon as the tensile failure value is reached in a finite element, it is deleted and all of its stress components are put to zero. The suppression of a finite element introduces a crack in the workpiece, making it possible for the chip to come off. All the workpiece get damage properties, again to avoid influencing and/or favouring the location where a crack will form.

The adopted criterion enhances the physical link with the real process thanks to the temperature dependency. It is nevertheless obvious that it can still be improved by making it also strain rate dependent for example.

The same mesh is used as for the ALE model.

4. Results

4.1. Chip morphology

The Ti6Al4V chip morphology from the reference article of Sun et al. [21] is presented in Fig. 5.

Fig. 6 shows chips produced by the three models. The first observation is that the Johnson–Cook law with a Lagrangian formalism (Fig. 6(a)) results in many highly deformed and undeleted elements and computing is quickly interrupted.[1] These elements are located close to the cutting edge radius of the tool. The suppression of this radius to get a sharp tool should reduce this problem. The finite edge radius of the tool is however one of the constraints imposed in the model's development and therefore it cannot be deleted.

The transition to TANH law and ALE formalism (Fig. 6(b)) produces a chip with slight teeth. Indeed they seem to fade away

[1] Continuous remeshing of the workpiece would have certainly led to a more satisfactory result. This possibility is unfortunately not available in Abaqus/Explicit v6.8.

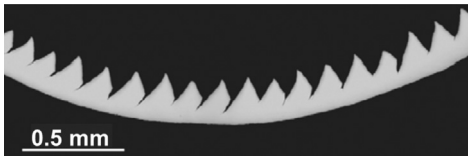

Fig. 5. Experimental Ti6Al4V chip from [21].

when the tool moves forward, because of the relative mesh movement. Finally, the combination of the Lagrangian formulation and the TANH law (Fig. 6(c)) produces a saw-toothed chip with a morphology similar to that obtained by Sun et al. [21].

The comparison of these three simulated chips shows that the one obtained with the LTANH model is the closest to the reference chip of Fig. 5.

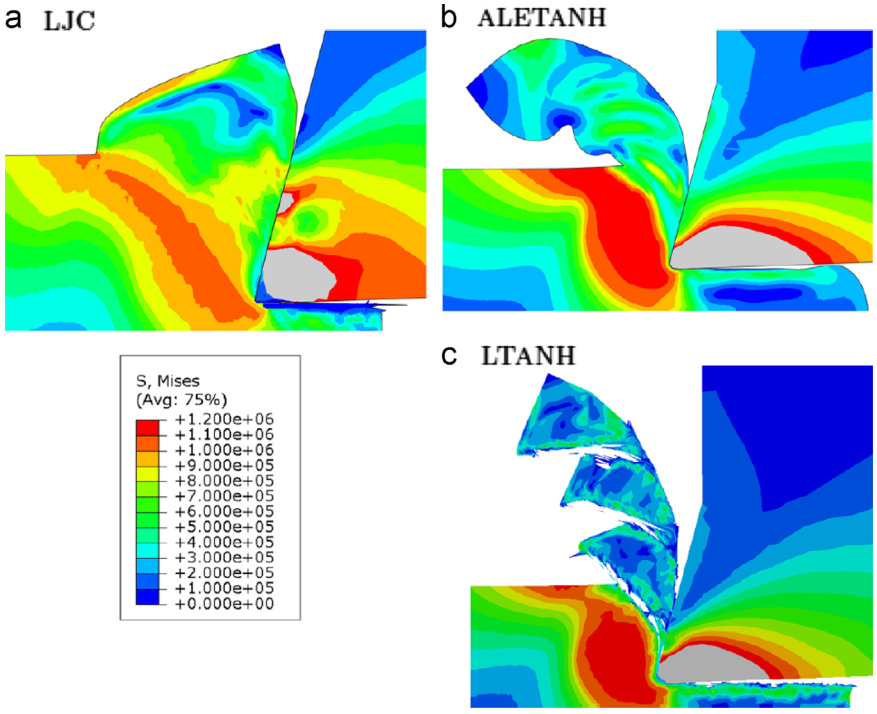

Fig. 6. Von Mises stresses contours (e^3 Pa) during chips formation (same chip length for the two models with TANH law).

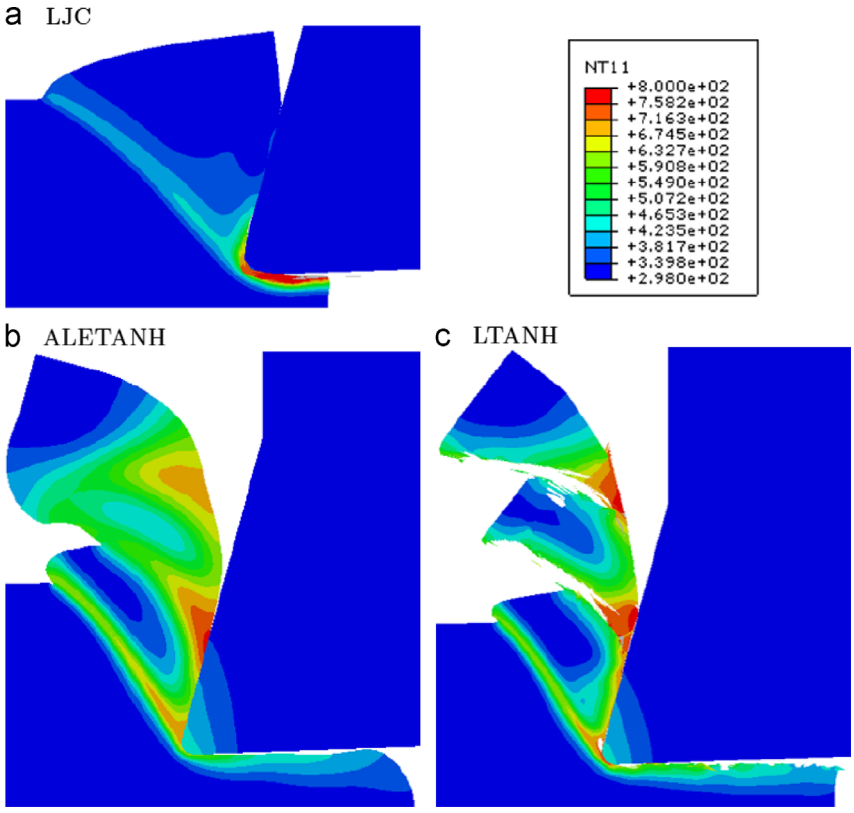

Fig. 7. Temperatures contours (in K) during chips formation.

Temperature contours are plotted in Fig. 7 for the three models. The large increase of temperature in the primary shear zone leading to the formation of the adiabatic shear band is clearly noticed. The temperature rise in the secondary shear zone is also observed.

Fig. 8 presents the chip obtained with a fourth model. It consists in the combination of the ALE formalism and the J–C behaviour law. Its purpose is to show that the J–C law allows us to form only a continuous chip. It is therefore not suitable to produce a saw-toothed chip.

4.2. Cutting forces

Cutting forces of the three models are presented and compared to the reference value of Sun et al. [21] in Fig. 9. This reference value is constant because it is the Root Mean Square (RMS) value of the measured signal.

Table 4 summarises the RMS force values for the three models and compares them to the experimental reference of Sun et al. [21]. This can be explained by the absence of strain softening in the Johnson–Cook law, contrary to the TANH law. As expected when looking at Fig. 9, the LJC model leads to the larger difference with the reference. The RMS value of the cutting force is quite close for both models with the TANH law. The cutting force of the ALETANH model is the closest to the reference of Sun et al. [21], which could be suspected as its evolution in Fig. 9 does not show severe drops under 175 N/mm, contrary to that of the LTANH models.

In Fig. 9, the LJC model exhibits a growing force, then it drops suddenly and remains approximately constant. Elements deletion could explain this force drop. The two models with the TANH law

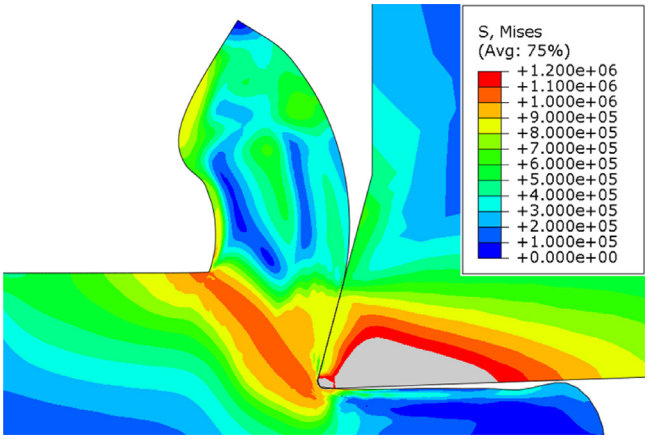

Fig. 8. Von Mises stress contours (e^3 Pa) during chip formation, ALE formalism and J–C law.

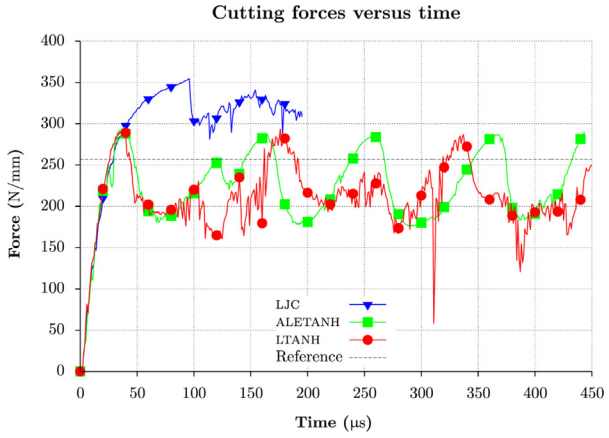

Fig. 9. Cutting forces (Reference: Sun et al. [21]).

Table 4
Comparison between modelled and experimental (from Sun et al. [21]) RMS cutting force values for the three models.

Source	RMS (N/mm)	Difference (%)
Sun et al. [21]	257	–
LJC (for ≈200 µs)	313	22
ALETANH (for ≈450 µs)	229	11
LTANH (for ≈450 µs)	216	16

lead to a similar cyclic evolution of the cutting force, typical of a saw-toothed chip, and the average values are close (slightly lower, as presented in Table 4) to the reference value of Sun et al. [21]. For the Lagrangian model the cyclic evolution can be linked to teeth formation. Indeed a drop in the cutting force corresponds to the production of a tooth. This drop is due to the formation of a shear band in the primary shear zone. The material is strongly softened therein, implying a large decrease in the force. The more rugged aspect of the force evolution of the LTANH model, when comparing to these of the ALETANH model, is caused by elements deletion in the first one. It can be seen as small impacts. In the ALE case each force drop corresponds to the formation of the disappearing teeth (some of which are still visible in Fig. 6(b)).

This, coupled with the chip morphologies, shows that the TANH law leads to a softening of the material allowing teeth (disappearing for ALETANH) formation. Consequently damage implementation is not a necessary condition for the formation of a numerical chip that is not continuous. It is noted, however, that taking it into account in the modelling (in LTANH model) leads to the formation of "real" teeth with a morphology close to the reference one, as already suggested by Calamaz et al. [16].

4.3. Link with the literature review

On the basis of the formalism and the constitutive law, it is concluded that the third model, LTANH, leads to the best results. Indeed the morphology produced is the closest to the reference one, the cutting force evolution is correlated with teeth formation and its value is very close to the reference value of Sun et al. [21]. It is now necessary to have a look at the chip formation mechanism to see if it is in accordance with the literature.

As presented previously three major theories are currently competing. The LTANH model considers that chip formation results of the combination of strain softening and crack propagation, which corresponds to the third theory presented in Section 2.3. The chip formation mechanism of this model will therefore be analysed and compared to the third theory from the literature.

According to this theory, high shear occurs in the primary shear band. Fig. 10(a) highlights the splitting of the shear band during the process, phenomenon noticed in the literature by Bäker et al. [6] and highlighted in Fig. 1. Another important feature of the chip formed is that the shear band is very narrow, indicating that the shear is actually highly localised (Fig. 10(b)). It is also observed that this shear band forms in two joining parts (Fig. 11(a)). Indeed, at first, it starts near the tool edge radius and propagates toward the free surface of the chip. Then, a second part starts from the free surface to the tool radius. The shear band is formed by their conjunction. In addition, the teeth are well marked and their formation is done via the propagation of a crack from free surface of the chip to the tool edge radius area (Fig. 11(b)). This crack turns into micro-cracks when approaching to the tool, in agreement with the literature.

It is therefore noted that this model adds to the morphology and the cutting force close to the experimental reference of Sun et al. [21] a chip formation mechanism incorporating the features highlighted in the literature.

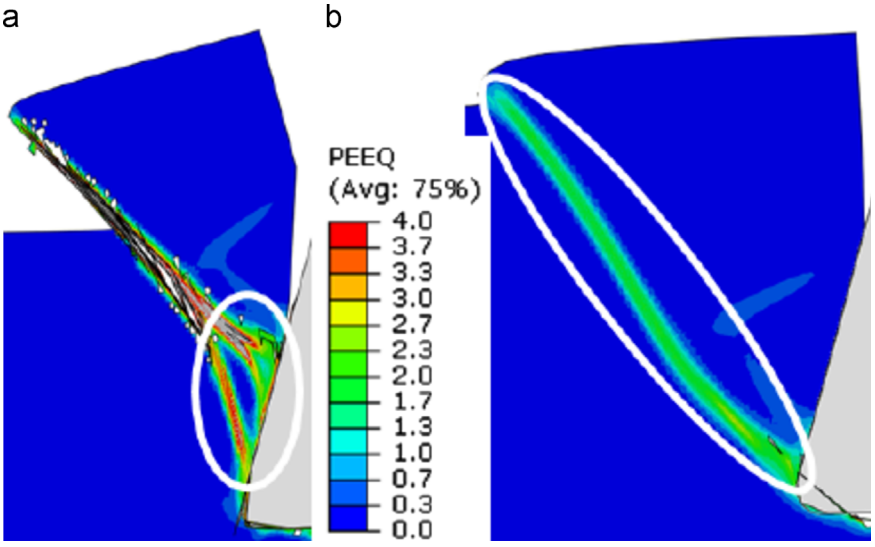

Fig. 10. Shear band (a) splitted and (b) narrow (LTANH, PEEQ: equivalent plastic strain).

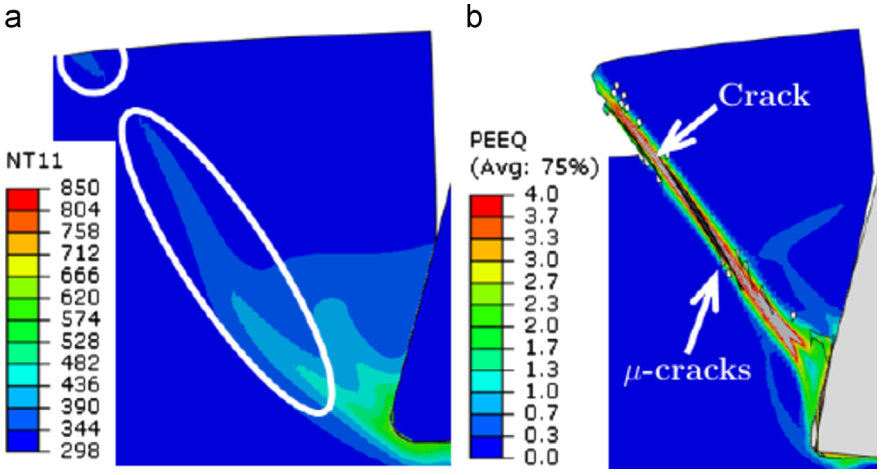

Fig. 11. Shear band (a) in two parts (b) with cracks and micro-cracks (LTANH, NT11: nodal temperature in K).

5. Results comparison with the literature reference

In this section a more advanced comparison is performed between modelling results and the reference of Sun et al. [21]. The model adopted is LTANH, combining the adiabatic shear band and the crack propagation, as its results are close to the experimental reference of Sun et al. [21].

5.1. Chip morphology comparison

Fig. 12 presents the chip (composed of six teeth completely formed and a seventh one in formation) after 1000 μs of simulation time. Different characteristics can be measured on a chip [16,11]: the distance between the end of two teeth, the distance between the end or the bottom of a tooth and the surface of the chip, the width of a tooth are some examples. Their major drawback is that their value is influenced by the curvature of the chip. It is therefore essential that the experimental chip to which the values obtained by modelling are compared has not been deformed! This is impossible to guarantee, especially due to the important experimental complexity to avoid the deformation of the chip.

The undeformed tooth length, L, highlighted in Fig. 12 is not influenced by the curvature of the chip. Sun et al. [21] measured a mean value for L of 0.13 mm on about 50 teeth. On the modelled chip this length could be measured on seven teeth. However it is not wise to take account of the first tooth, as the cutting tool is just entering into the workpiece and the contact surface is vertical (in a certain way it can be seen as a "cutting regime" not yet established).

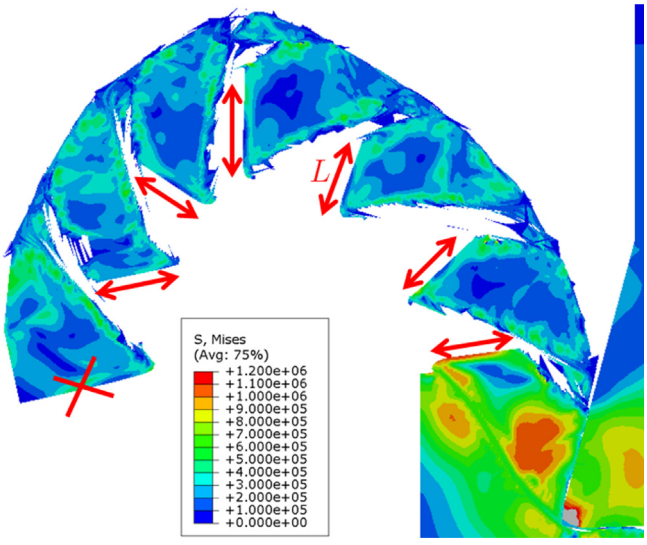

Fig. 12. Modelled chip (Von Mises stresses (e^3 Pa)).

The mean value measured on the six following teeth is equal to 0.159 mm. The modelled chip has thus slightly longer teeth (about 20%) than the reference chip.

When comparing the numerical chip and the experimental one, it is observed that, while the global morphology and the undeformed tooth length are close, the crack is longer and wider for the model than for the experimental chip. The chip separation criterion could be considered as a parameter that could be modified to reduce this drawback concerning the chip morphology. As presented in Section 3.5.2, this criterion is based on the temperature dependent tensile failure of Ti6Al4V and it could be improved to make it also strain rate dependent for example. In this paper the authors have chosen not to modify the failure curve and thus to use the "original" data provided in Ref. [31]. This aspect of the model has been studied for another cutting speed value more in detail in [37].

Morphologies for other cutting conditions from Sun et al. [38] were also considered. Saw-toothed (v_c=80 m/min, h=0.163 mm) and nearly continuous (v_c=6 m/min and v_c=14 m/min, h=0.19 mm) chips were obtained with numerical morphologies qualitatively close to the experimental ones as presented in Fig. 13. The purpose here is to confirm that the model is able to deal with other cutting conditions, leading for example to chips that are not saw-toothed. Fig. 13 shows that it is fulfilled.

5.2. Cutting forces comparison

The forces evolution shown in Fig. 14 is cyclic, which was expected and already highlighted in Fig. 9. It is noticed that the cutting force presents seven maxima corresponding to the seven teeth formed (the seventh one being in formation).

Table 5 presents a comparison of RMS values of modelled and measured (by Sun et al. [21]) forces. Force magnitudes are of the same order and the cutting force is closer to the reference than the feed force, as expected from Fig. 14.

The choice of the parameters of the material constitutive model influences the value of the forces modelled, as highlighted by Calamaz et al. [16] for TANH law and Ti6Al4V and Umbrello et al. [39] for J–C law and AISI 316L. Moreover the thermal treatments applied to the machined material influence the cutting forces and the parameters of the behaviour law. Differences in the Ti6Al4V state from

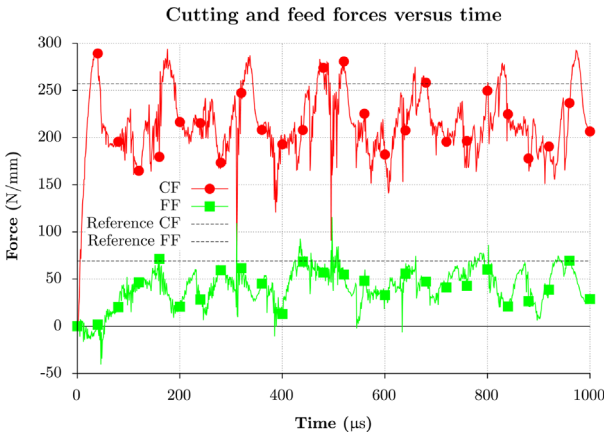

Fig. 14. Cutting force (CF) and feed force (FF) versus time.

Table 5
Comparison between modelled (for around 1000 µs) and experimental (from Sun et al. [21]) RMS force values.

Force	Sun et al. [21] (N/mm)	Modelling (N/mm)	Difference (%)
Cutting force	257	218	15
Feed force	69	46	33

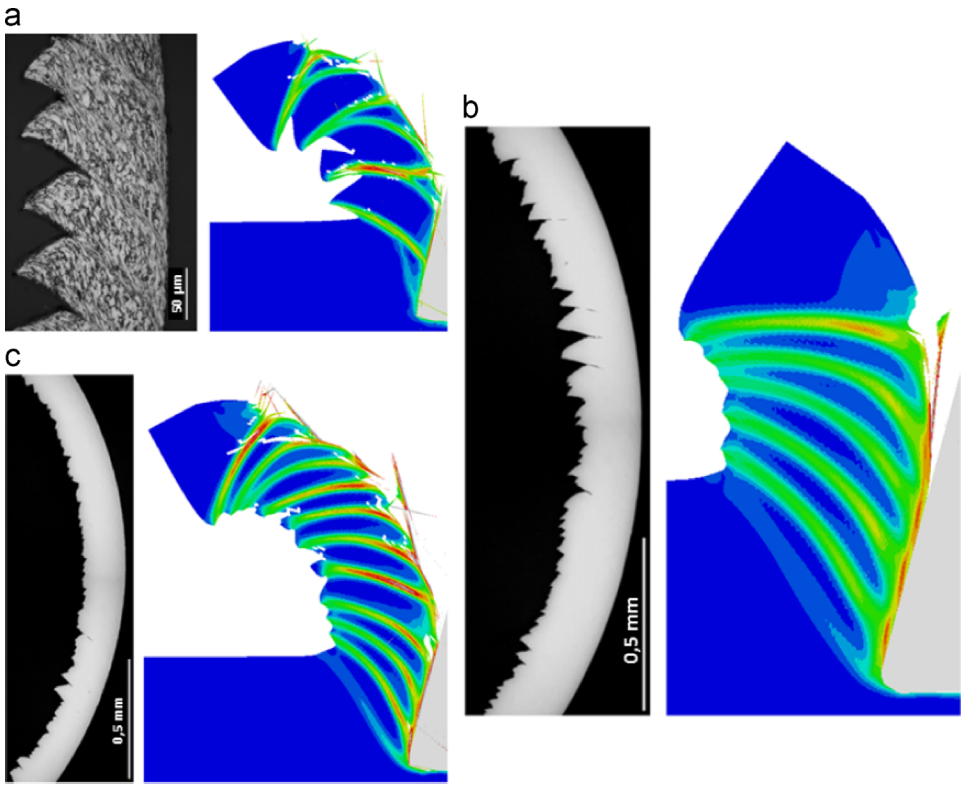

Fig. 13. Chip morphologies for other cutting conditions, experiments from Sun et al. [38]: (a) v_c=80 m/min and h=0.163 mm, (b) v_c=6 m/min and h=0.19 mm and (c) v_c=14 m/min, h=0.19 mm.

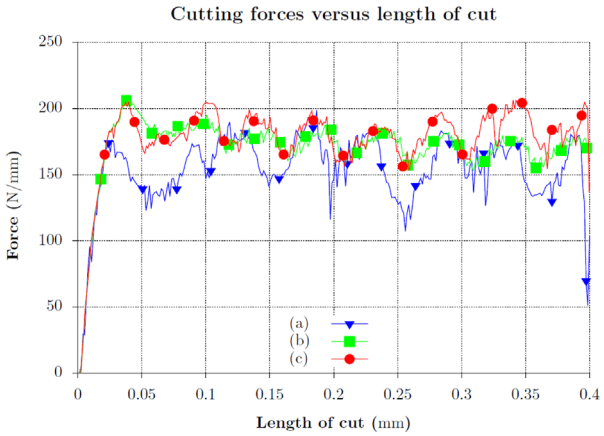

Fig. 15. Cutting forces versus length of cut for the three other cutting conditions, (a) v_c=80 m/min and h=0.163 mm, (b) v_c=6 m/min and h=0.19 mm and (c) v_c=14 m/min, h=0.19 mm.

the experiments of Sun et al. [21] and from the TANH law identification of Calamaz et al. [16] are highly probable and contribute to the differences observed in Table 5. As for the failure curve (cf. Section 5.1), the authors have chosen to work with the "original" TANH law given by Calamaz et al. in their article [16]. The influence of the material behaviour law on the results of the model is studied in [37] (for another cutting speed) and the behaviour law is modified to improve the accuracy of the modelled cutting forces.

Fig. 15 presents the cutting forces for the three cutting conditions introduced in Section 5.1. They are plotted versus the length of cut and not versus time as usually. Indeed the large difference between the cutting speeds of the three cases (from 6 m/min to 80 m/min) does not allow us to compare them versus time on the same graph. In their article, Sun et al. [38] do not provide the RMS cutting force values for these cutting conditions. The authors have therefore no experimental value to plot with their simulation results. This is however not a limitation as only a qualitative comparison of the morphologies of the chips is performed, in order to show that the model is able to give good chip morphologies for other cutting conditions.

For v_c=80 m/min and h=0.163 mm, the cutting force variations are large, as expected when looking at the saw-toothed chip morphology in Fig. 13. This figure also shows that the two other cutting conditions lead to a nearly continuous chip. The result on the cutting force is, as expected, variations of smaller amplitudes. These slight force variations are due to the "ripples" on the free chip surface. Concerning the forces level, as the depth of cut is larger and the cutting speeds are lower for the (b) and (c) cutting conditions, it was expected to obtain higher cutting forces than for the first (a) cutting conditions, which is clearly observed in Fig. 15. It qualitatively confirms that the model developed is able to deal with various cutting conditions.

5.3. Teeth formation frequency estimation

Besides the chip morphology, the teeth formation frequency is an important parameter in the comparison between reference and modelled chips, as it takes into account the dynamics of the chip formation. The teeth considered for this estimation are the six teeth used for the comparison of the chip morphology. This frequency can be achieved in several ways:

- Based on chip geometry.
- Based on forces:
  - Estimation from forces evolution.
  - Fast Fourier Transform (FFT) of the forces signal. It will not be used in this case as the duration of the modelled cutting process is very short.[2]
  - Best sine in a least squares way fitted on forces evolution.

Up to now very few informations can be found on numerical studies about teeth formation frequency and its method of calculation. This estimation is therefore an important contribution of this study.

5.3.1. Estimation based on the chip geometry

The teeth formation frequency can be estimated from the undeformed tooth length. This frequency, F_g, is given by [21]

$$F_g = \frac{v_c}{L} \tag{3}$$

with v_c the cutting speed (75 m/min).

The teeth formation frequency resulting from the mean tooth length measured by Sun et al. [21] is 9615 Hz and 7862 Hz for the modelling. The difference between the two frequencies is 18%.

The order of magnitude of measured and simulated values is identical, confirming that the model leads to a saw-toothed Ti6Al4V chip close to the reference chip, and its dynamic of formation is as well. The small difference could be partially explained by the number of teeth from the model much lower than the reference. The few teeth used in this case are much less representative than all these that have been measured (6 versus about 50) and the influence of each on the average value is greater.

5.3.2. Estimation based on the cutting force evolution

It has been estimated that the first tooth was formed in 116 µs. Therefore about 884 µs are required for the formation of the six teeth composing the chip (six maxima are identified in this interval of time on the cutting force evolution). The formation frequency F_e is therefore roughly estimated by

$$F_e = \left(\frac{884 \times 10^{-6}}{6}\right)^{-1} = 6787 \text{ Hz} \tag{4}$$

This value is of the same order of magnitude as the reference one (9615 Hz), although lower. The difference equals almost 30%.

5.3.3. Estimation based on the least squares method

The forces evolution can be regarded as a sine of frequency equals to that of the teeth formation and whose DC component corresponds to the average force value. Following this observation, this paragraph proposes to adjust the best sine in a least squares sense to the forces signal.

Fig. 16 presents this sine adjusted relative to the cutting force. It presents a DC component (zero shift) of 215 N/mm, an amplitude of 26 N/mm and a frequency of 6402 Hz. The same fitting is done on the feed force evolution. Its DC component is 45 N/mm, its amplitude is 11 N/mm and its frequency is 6031 Hz.

Again, the average forces value is close to the RMS reference value. The difference for the teeth formation frequency based on the cutting force is 33%, while it is 37% for the feed force. The two forces result in slightly (about 6%) different frequencies, as their evolution might suggest.

5.3.4. Conclusions of the teeth formation frequency estimation

The three methods lead to teeth formation frequencies of the same order of magnitude as Ref. [21]. These simulated frequencies are all smaller than the reference. The geometric method, simple

[2] For the six teeth, the frequency resolution is of the order of 1150 Hz, which is not good enough for a correct estimation.

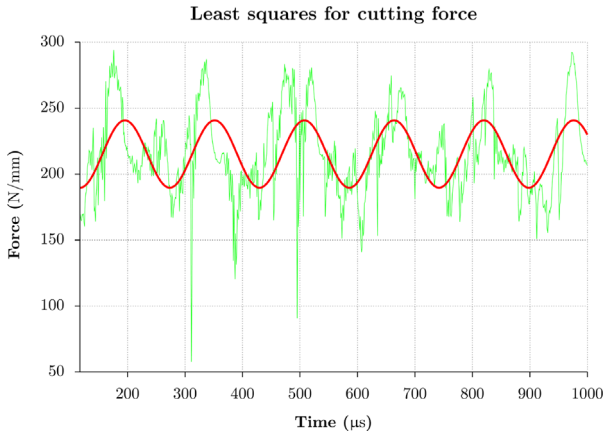

Fig. 16. Best sine in the least squares sense for cutting force.

to implement in a modelling context, leads to the nearest value. The method involving the least squares results in different frequencies for the two forces, which could be suspected because of their evolution.

The model can then produce a saw-toothed Ti6Al4V chip with formation dynamics close to the experimental reference chip.

6. Conclusions

The formation of a saw-toothed Ti6Al4V chip is still an ongoing problem in the literature (in terms of physical phenomena and modelling) in which three different theories are found. Three finite element models have been developed to produce such a chip.

The modelling results allow us to position ourselves in relation to the literature concerning the process and physical phenomena occurring during the formation of a saw-toothed chip. It turns out that the theory coupling the adiabatic shear band and the crack propagation seems the most likely. The adiabatic shear band results in material softening due to severe localised deformation and is the damage precursor. Then a crack starts from the free surface of the chip and propagates towards the tool in turning into micro-cracks. The model containing all the characteristics necessary for such a process is the LTANH Lagrangian model using the TANH law, a modified Johnson–Cook law. It shows that taking account of the thermal softening of the material is not sufficient and that its strain softening must also be considered.

So far, few authors [5,6,16] present a model producing a saw-toothed chip with a morphology similar to that observed experimentally and with a number of teeth greater than one or two. Using a physical chip separation criterion without numerical tricks to influence the chip formation and taking into account the tool edge radius is still not widespread also not taking the physics of the chip formation into account.

This study shows that taking account of the thermal softening of Ti6Al4V is not sufficient to form a saw-toothed chip as the strain softening must also be considered in the behaviour law. The TANH law should therefore be used in finite element modelling of Ti6Al4V orthogonal cutting instead of the J–C law, as suggested by Calamaz et al. [16] and Sima and Özel [19], regardless of the finite element software used.

Finally, as this model has not been developed for a determined set of cutting conditions and as numerical tricks have been avoided, it can be used in many other cutting conditions (to study the influence of the depth of cut on chip formation for example [40]).

References

[1] Destefani J. Introduction to titanium and titanium alloys, properties and selection: nonferrous alloys and special-purpose materials, vol. 2. ASM Handbook; 1990.
[2] Barry J, Byrne G, Lennon D. Observations on chip formation and acoustic emission in machining Ti–6Al–4V alloy. Int J Mach Tools Manuf 2001;41:1055–70.
[3] Molinari A, Musquar C, Sutter G. Adiabatic shear banding in high speed machining of Ti-6Al-4V: experiments and modeling. Int J Plast 2002;18:443–59.
[4] Owen D, Vaz M. Computational techniques applied to high-speed machining under adiabatic strain localization conditions. Comput Methods Appl Mech Eng 1999;171:445–61.
[5] Fourment L, Delalondre F. A 3D study of the influence of friction on the Adiabatic Shear Band formation during High Speed Machining. In: Proceedings of the ESAFORM2008 conference; 2008.
[6] Bäker M, Rosler J, Siemers C. A finite element model of high speed metal cutting with adiabatic shearing. Comput Struct 2002;80:495–513.
[7] Komanduri R, Turkovich BV. New observations on the mechanism of chip formation when machining titanium alloys. Wear 1981;69:179–88.
[8] Komanduri R. Some clarifications on the mechanics of chip formation when machining titanium alloys. Wear 1982;76:15–34.
[9] Hou Z, Komanduri R. Modeling of thermomechanical shear instability in machining. Int J Mech Sci 1997;39:1279–314.
[10] Vyas A, Shaw MC. Mechanics of saw-tooth chip formation in metal cutting. J Manuf Sci Eng 1999;121:163–72.
[11] Hua J, Shivpuri R. Prediction of chip morphology and segmentation during the machining of titanium alloys. J Mater Process Technol 2004;150:124–33.
[12] Castro LR. Identification des sources de vibration en usinage, Etude expérimentale et numérique [Ph.D. thesis]. Université Paul Verlaine, Metz; 2006.
[13] Bai Y, Dodd B. Adiabatic shear localisation: occurrence, theories and applications. Pergamon Press; 1992.
[14] Giovanola H. Adiabatic shear banding under pure shear loading. Part II: fractographic and metallographic observation. Mech Mater 1988;7:73–87.
[15] Seshacharyulu T, Medeiros S, Morgan J, Malas J, Frazier W, Prasad Y. Hot deformation and microstructural damage mechanisms in extra-low interstitial (ELI) grade Ti–6Al–4V. Mater Sci Eng A 2000;279:289–99.
[16] Calamaz M, Coupard D, Girot F. A new material model for 2D numerical simulation of serrated chip formation when machining titanium alloy Ti-6Al-4V. Int J Mach Tools Manuf 2008;48:275–88.
[17] Calamaz M. Etude des mécanismes d'endommagement des outils carbure WC-Co par la caractérisation de l'interface outil-copeau – Application à l'usinage de l'alliage de titane aéronautique TA6V [Ph.D. thesis]. Université de Bordeaux; 2008.
[18] Calamaz M, Coupard D, Girot F. Numerical simulation of titanium alloy dry machining with a strain softening constitutive law. Mach Sci Technol: Int J 2010;14:244–57.
[19] Sima M, Özel T. Modified material constitutive models for serrated chip formation simulations and experimental validation in machining of titanium alloy Ti-6Al-4V. Int J Mach Tools Manuf 2010;50:943–60.
[20] Johnson G, Cook W. A constitutive model and data for metals subjected to large strains, high strain rates and high temperatures. In: Proceedings of the seventh international symposium on ballistics. The Hague, The Netherlands; 1983. p. 541–7.
[21] Sun S, Brandt M, Dargusch M. Characteristics of cutting forces and chip formation in machining of titanium alloys. Int J Mach Tools Manuf 2009;49:561–8.
[22] Ducobu F. Contribution à l'étude de la formation du copeau de Ti6Al4V en coupe orthogonale. Approches numérique et expérimentale pour la compréhension des mécanismes de coupe macroscopique et microscopique (Contribution to the study of Ti6Al4V chip formation in orthogonal cutting. Numerical and experimental approaches for the comprehension of macroscopic and microscopic cutting mechanisms) [Ph.D. thesis]. University of Mons (UMONS), Faculty of Engineering (FPMs); 2013.
[23] Meyer HW, Kleponis DS. Modeling the high strain rate behavior of titanium undergoing ballistic impact and penetration. Int J Impact Eng 2001;26:509–21.
[24] Özel T, Zeren E. Numerical modelling of meso-scale finish machining with finite edge radius tools. Int J Mach Mach Mater 2007;2:451–768.
[25] Goeffers E. Simulation numérique de la formation du copeau et détermination des efforts de coupe en fraisage du Ti6Al4V [Master's thesis]. Faculté Polytechnique de Mons, Mons; 2008.
[26] Sun J, Guo YB. Material flow stress and failure in multiscale machining titanium alloy Ti–6Al–4V. Int J Adv Manuf Technol 2009;41:651–9.
[27] Lesuer DR. Experimental investigations of material models for Ti–6Al–4V Titanium and 2024-T3 Aluminum. Technical Report. Lawrence Livermore National Laboratory; 2000.
[28] Pantalé O. Plateforme de prototypage virtuel pour la simulation numérique en Grandes Transformations Thermomécaniques Rapides. Technical Report. Institut National Polytechnique de Toulouse; 2005.
[29] Ding R, Guo Z, Wilson A. Microstructural evolution of a Ti–6Al–4V alloy during thermomechanical processing. Mater Sci Eng A 2002;327:233–45.
[30] Lee W, Lin C. High-temperature deformation behaviour of Ti6Al4V alloy evaluated by high strain-rate compression tests. J Mater Process Technol 1998;75:127–36.

[31] Lampman S. Wrought titanium and titanium alloys, Properties and selection: nonferrous alloys and special-purpose materials, vol. 2. ASM Handbook; 1990.
[32] Nasr M, Ng E-G, Elbestawi M. Effects of workpiece thermal properties on machining-induced residual stresses—thermal softening and conductivity. Proc Inst Mech Eng B: J Eng Manuf 2007;221:1387–400.
[33] Woon K, Rahman M, Fang F, Neo K, Liu K. Investigations of tool edge radius effect in micromachining: a FEM simulation approach. J Mater Process Technol 2007;167:316–37.
[34] Mabrouki T, Girardin F, Asad M, Rigal J-F. Numerical and experimental study of dry cutting for an aeronautic aluminium alloy (A2024-T351). Int J Mach Tools Manuf 2008;48:1187–97.
[35] HKS. Abaqus Analysis User's Manual, Version 6.8, Dassault Systèmes, 2008.
[36] Lorentzon J, Jarvstrat N, Josefson B. Modelling chip formation of alloy 718. J Mater Process Technol 2009;209:4645–53.
[37] Ducobu F, Rivière-Lorphèvre E, Filippi E. Influence of the material behavior law and damage value on the results of an orthogonal cutting finite element model of Ti6Al4V. Proc CIRP 2013;8:378–83.
[38] Sun S, Brandt M, Dargusch M. Machining Ti–6Al–4V alloy with cryogenic compressed air cooling. Int J Mach Tools Manuf 2010;50:933–42.
[39] Umbrello D, M'Saoubi R, Outeiro J. The influence of Johnson–Cook material constants on finite element simulation of machining of AISI 316L steel. Int J Mach Tools Manuf 2007;47:462–70.
[40] Ducobu F, Rivière-Lorphèvre E, Filippi E. A Lagrangian FEM model to produce saw-toothed macro-chip and to study the depth of cut influence on its formation in orthogonal cutting of Ti6Al4V. Adv Mater Res 2011;223:3–11.